Bos Taurus (A-2) Urine Assisted Bioactive Cobalt Oxide Anchored ZnO: A Novel Nanoscale approach

Omkar S. Karvekar
Shivaji University
Apurva S. Vadanagekar
Shivaji University
Prashant Sarvalkar
Shivaji University
Sarita Jadhav
Shivaji University
Richa Singhan
Shivaji University
Suresh Suryawanshi
Shivaji University
Jyoti Jadhav
Shivaji University
Kiran Kumar Sharma
Shivaji University
Neeraj Prasad (neeraj_prasad21@rediffmail.com)
Shivaji University

Article

Keywords: Biomimetic nanotechnology, Co3O4 NPs, Nanocomposite, Biological Activity, Antibacterial

Posted Date: July 27th, 2022

DOI: https://doi.org/10.21203/rs.3.rs-1849967/v1

Abstract

Biomimetic nanotechnology is a fast-growing technology with far-reaching implications in a variety of therapeutic applications. The goal of this research is to develop green, environmentally friendly, and cost-effective strategies for producing cobalt oxide (Co_3O_4) nanoparticles from *Bos Taurus Indicus* (A-2) urine and zinc oxide nanorods from the hydrothermal process. A solid-state reaction process is used to make nanocomposite materials. The synthesized nanomaterials and composites were characterized using advanced characterization techniques such as XRD, FE-SEM with EDS, DLS, Zeta potential, FT-IR, Raman spectroscopic analysis, and TGA with DSC analysis. The anti-bacterial, Anti-oxidant and anti-inflammatory effects of the synthesized nanomaterials and composites were investigated. This implies that they might be beneficial in medicine and drug administration.

Introduction

The study of material properties at the nanoscale is the focus of nanoscience and technology. Richard Feynman, a renowned physicist, pioneered the concept of nanotechnology in 1959. Then, after extensive research in the fields of nanoscience and technology, nanotechnology deals with the synthesis and application of materials at nanometer scale. In diverse areas like electrochemical application [1], sensors [2], photocatalysis [3], electronics [4], toxic chemical reduction [5,6], medical diagnosis [7], cosmetics [8], textile [9], veterinary sciences [10], and are becoming more attractive as novel uses, from medical diagnostics to gene therapy vehicles etc.

For the past two decades, researchers from diverse fields have attempted to manufacture nanomaterials using several synthetic processes. Materials' characteristics at the nanoscale differ from those in the bulk. This is due to the large surface area, inefficient gravitational forces, and effective van der wall's force of attraction. Physical, chemical, or biological approaches can be used to synthesize NPs. Physical and chemical approaches are restricted by complex processes that need the use of expensive instruments as well as toxic byproducts [9,10]. As a result, nanoscience and technology researchers attempted to establish a cost-effective alternative approach for producing defect-free nanomaterials. Later, it was determined that the chemical method of synthesis is not ecologically friendly, so a group of researchers developed a biological approach of synthesis of nanoscale materials. Biological methods of synthesis have grown in popularity among academics during the last 15 years. The researchers were able to effectively generate a large number of transition metal nanoparticles using a biological method. Previously, researchers employing the biological way of synthesis employed microorganisms such as fungus and bacteria, as well as other plant extracts, to synthesize nanoscale materials [9,11]. The use of microorganisms to synthesize nanoparticles was a costly job that also needed aseptic settings. Previously, various plant components containing metabolites, such as leaves, fruits, stems, roots, bark powder, and seeds, were used as reducing and capping agents. Our goal was to create nanomaterials at the lowest possible cost and with the fewest resources available in the laboratory. The authors then had an epiphany: why not employ animal metabolic waste, such as cow urine, to generate nanoscale materials? The authors were inspired by Ayurveda, an ancient Indian medical practice. Cow urine's multiple medicinal advantages are widely documented in Ayurvedic literature [12].

According to Ayurvedic literature, cow urine has anti-neoplastic properties. According to laboratory examination, cow urine includes minerals such as iron, copper, nitrogen, manganese, silicon, magnesium, calcium salts, mineral salts, enzymes, and vitamins such as A, B, C, D, E, uric acid, and other hormones [6]. According to ancient Ayurvedic literature, cow urine can heal leprosy, peptic ulcers, liver illnesses, renal disorders, asthma, psoriasis, anemia, some types of allergies, and cancer. The authors have first-hand knowledge of the laxative qualities of Indian cow urine [13].

Thus, our research group has synthesized various transition metal and metal oxide NPs like cadmium oxide [14], palladium [15], copper oxide [16], and silver [6] using Indian cow urine. These nanoparticles, which were synthesized using Indian cow urine, have strong biological and catalytic properties. Biological approaches based on Indian cow urine appear to be the most simple, cost-effective, fast, non-toxic, and ecologically friendly of the methods studied. According to current medicine, cobalt isotopes have anti-neoplastic properties. As a result, we attempted to combine the two, namely, cow urine for the production of cobalt

oxide nanoparticles (Co_3O_4 NPs) and hydrothermally synthesized ZnO nanorods (NRs). Metal NPs and nanocomposites are attracting researchers from all over the world due to their superior electrical, magnetic, optical, and biological capabilities. In this study, we synthesize Co_3O_4 NPs from *Bos Taurus Indicus* urine and ZnO NRs using a hydrothermal approach and investigate their combined effect against various bacteria and fungi.

Experimental Section

Materials. Ammonia Solution (30 wt%), Cetyl Trimethyl Ammonium Bromide (CTAB), Cobalt (II) Chloride Hexahydrate ($CoCl_2.6H_2O$), Zinc Nitrate Hexahydrate (Zn $(NO_3)_2.6H_2O$) chemicals are procured form Sigma-Aldrich, Milwaukee (USA). The liquid metabolic waste of a 7-year-old healthy adult female Bos taurus indicus is utilized in the production of nanomaterials. With the agreement of the animal rearer, liquid metabolic waste from a cow farm in Kaneri village, Kolhapur, India (16.6237° N, 74.2722° E) is collected. The freshly discharged cow's liquid metabolic waste was collected in a clean screw-capped reagent bottle. Using Whatman filter paper (grade no. 3), the liquid metabolic waste from Gir cows was dribbled and stored at 5^oC for further experimentation.

Microbes namely *Escherichia coli* (NCLM2832), *Bacillus cereus* (NCLM2703), *Staphylococcus aureus* (NCLM2602) and *Salmonella typhimurium* (NCLM2501) procured from National Chemical Laboratory Pune were used for this study. The stock cultures were maintained on nutrient agar slants at 37ºC. DPPH (2,2-diphenyl-1-picrylhydrazyl), ABTS (2,2'-azino-bis (3-ethyl benzothiazoline -6- sulfonic acid)), BSA (bovine serum albumin) and All other chemicals required for the experiments were of analytical grades and purchased from Sigma (St Louis MO, USA).

Biomimetic-Synthesis of Co_3O_4 NPs. The liquid metabolic waste discharge of fully vaccinated, healthy and 7 years old *Gir* cow was collected in fresh glass stoppered bottle and immediately brought to laboratory for experimentation process.

Cobalt (II) Chloride was procured from Sigma Aldrich and used without further purification. Then we prepared a 0.1 M $CoCl_2.6H_2O$ solution in 100 mL of distilled water. In order to stabilize the NPs, a cationic surfactant, CTAB (0.1% w/v), was used. Then solution was kept on magnetic stirrer. Then cow urine was added dropwise in the beaker containing cobalt (II) chloride solution. After addition of sufficient amount of cow urine (i.e. 25 mL) in the cobalt (II) chloride solution whitish brown colored precipitate appeared in the solution.

Bos taurus Indicus (A-2) urine contains urea and it acts as a reducing, binding, and capping agent in this reaction. CTAB provides additional stability. When cow urine reacts with Co^{2+} ions, it gets converted into Co^0. Thus, there is formation of Co_3O_4 NPs. Once the Co_3O_4 nanomaterials are formed in the solution, it was centrifuged and the precipitate was separated and dried. Then the dried precipitate was kept in the furnace for about 2 hrs at 900°C for annealing. Then the final product, which appeared dark blue in color, was collected and milled using the mortar and pestle into the fine granular powder. Lastly, synthesized material was stored and used for further purposes like characterizations and applications.

Plausible Mechanism of Action. The literature survey reveals that liquid metabolic waste of *Bos taurus Indicus* (A-2) cow contains urea, creatinine, aurum hydroxide, carbolic acid, phenol, calcium and magnesium. After photo activation few biogenic volatile inorganic and organic compounds like CO_2, NH_3, CH_4 methanol, propanol, acetone and some secondary nitrogenous products are also formed. The possible reaction mechanism for the Co_3O_4 NPs is given below:

The chemical formula of urea is $CO(NH_2)_2$. Here the carbonyl group, i.e. C=O, is directly connected to two $–NH_2$ groups. Actually, due to the presence of a lone pair of electrons on the nitrogen atom, urea seems to be a base. However, because of electronegative character of carbonyl group it behaves as a neutral molecule. However, when urea is treated with the enzyme urease or at a high temperature, urea is converted to ammonia through hydrolysis. Urea is broken down into ammonia and isocyanate ions as a byproduct in the first step of the reaction. At pH levels of less than 5 and greater than 12, this reaction is reversible. Isocyanate is hydrolyzed to form ammonia in the second step (Shown in Fig. 1a), and carbon dioxide is produced

as a byproduct. The rate of urea hydrolysis is faster at 35°C than at 15°C. The pH impact is only noticeable between pH 6 and pH 8[6].

According to another conception, the chemical composition affirms cow urine contains Allantoin ((2,5-Dioxo-4-imidazolidinyl) urea), creatinine(2-Amino-1-methyl-5H-imidazol-4-one), and uric acids (7,9-Dihydro-1H-purine-2,6,8(3H)-trione). The bio-inspired synthesis of Co_3O_4 NPs using Indian *Gir* cow urine can be explained as metal ions come in contact with various biomolecules present in cow urine (shown in fig. 1b) [17].

Hydrothermal Synthesis of ZnO Nanorods (NRs). Morphology of zinc oxide nanomaterial depends upon its route of synthesis, concentration of precursor, nature of capping agent, reaction temperature etc. ZnO NRs were synthesized through hydrothermal technique. 0.2 M Zinc nitrate solution was prepared by dissolving the precursor in distilled water. 200 ml of Zinc nitrate solution was taken in a 500 ml capacity borosilicate made beaker. A magnetic needle was inserted in the beaker and is kept on magnetic stirrer. The magnetic needle was rotated with high speed around 700 rpm. Meanwhile, the burette was filled with 30 wt% ammonia solution, which was then dropped into the beaker while continuously stirring. Initially, a white precipitate was formed. However, after the addition of a few drops of ammonia, the solution turned colorless. When the solution became colorless, the ammonia addition was stopped, and the solution was transferred to an autoclave for hydrothermal treatment at 120^oC for 90 minutes. When the system was cooled to room temperature, the resultant product was collected and washed twice with distilled water followed by ethanol. In addition, the product was dried using the air-drying method at room temperature for a 2-hour time period, followed by a furnace for about 2 hours at 450 °C for annealing. It was stored for further use[3].

Preparation of nanocomposites. At the end of above experimentations, we are getting cobalt oxide and zinc oxide in Nano form. The Nano composite can be synthesized by grinding these two Nano materials with the help of mechanical ball milling technique. For the synthesis of Nanocomposite desired proportion of Co_3O_4 and ZnO Nanomaterials were taken in mortar and finely grinded for about 3 hours with pestle. Here we employed the method same as used in mechanical ball milling or solid-state reaction. We tried to synthesize two composite materials with different proportions of Co_3O_4. We synthesized 5% w/w Co_3O_4 NPs and ZnO NRs Nano-composites (Co 5%) and 10% w/w Co_3O_4 NPs and ZnO NRs Nano-composite (Co 10%) materials. The mixture was taken in the mortar and milled smoothly for about 3 hours. In the synthesized composite material, there no primary bonds like ionic, covalent or metallic. Disparately due to secondary bonds like van der wall's some weak attractive and repulsive forces are observed between Co_3O_4 NPs and ZnO NRs.

Characterization Study. After successfully synthesis of nanomaterial it becomes very important to ensure their size, shape, surface charge and morphology etc. As the materials at nanoscale are beyond the perception of human eyes, we require advance characterization techniques to reveal it.

The products were characterized by simultaneous thermal analysis, X-Ray Diffraction, scanning electron micrographs etc. To illustrate the crystalline structure of the Co_3O_4 NPs, ZnO NRs and Co_3O_4-ZnO nanocomposites X-ray diffractometer equipped with irradiation line Kα of copper (Bruker D8 advanced, Germany) was used to record the XRD spectrum and their corresponding size was calculated using Sherer equation. Furthermore, Field Emission Scanning Electron Microscope is used for study of surface morphology of the nanomaterials, here used TESCON MIRA-3 field emission-scanning electron microscope (FESEM) equipped with an Energy Dispersive Spectroscopy (EDS) detector to characterized Co_3O_4 NPs, ZnO NRs and Co-ZnO nanocomposites. The in-situ investigation of the interface was done using FT-IR, which revealed diverse functional groups adsorbed on the synthesized nanomaterials. The material was put on KBr pellets and we used an ALPHA Bruker FT-IR spectrometer. When using a Ranishaw Raman spectroscope, the Raman analysis ranges from 100 to 3200 cm^{-1}. The particle size and charge both were analyzed using Nano ZS 90 (Malvern, UK).

Biomedical potential of Nanoparticles

Minimal inhibitory concentration (MIC). The antibacterial potential of synthesized Co_3O_4 NPs, ZnO NRs and nanocomposites of both was evaluated by MICs [18]. The stocks of (1 mg/ml) nanomaterials were used after solicitation, whereas different working solutions of nanomaterials (50, 100, 150 and 200 µg/mL) were made. In this experiment, new inoculums of gram-positive and gram-negative bacterial strains were used. All bacterial strains were inoculated individually in 100 mL of various nanomaterial concentrations and cultured for 20–24 hours in a shaking incubator (REMI) at 100 rpm at 37^{o}C, using a UV-Vis spectrophotometer, we evaluated the absorbance of each tube at 625 nm to see if microbial growth was inhibited or stimulated. A negative control as distilled water was maintained along with positive control of Streptomycin and Fluconazole (as standard reference substances) for antibacterial and antifungal potential respectively at concentration of 1 mg/mL. MIC were defined as the lowest nanomaterial's concentrations at which growth of bacterial cells were inhibited.

Agar well diffusion method for Antibacterial and Antifungal potential. The antibacterial and antifungal activities of the compounds are assessed using the standard agar well diffusion technique. With slight modifications, standard agar well diffusion procedures were used to determine the antibacterial efficiency of Co_3O_4 NPs and ZnO NRs against four distinct microorganisms [19]. 100 mL of different nanomaterial concentrations were placed into wells on agar plates, which were then kept at 4°C for 30–40 minutes before being moved to an incubator for overnight storage at 37°C.The plates were observed the inhibitory zones were seen after 48 hours. After this medium range antibiotic Streptomycin of concentration 100µg/mL was used as reference substance.

In Similar consent the PDA plates were prepared using submerged inoculation of two fungal strains: *Aspergillus niger* and *Fusarium solani* JALPK [20]. The different concentration of nanomaterials concentrations was introduced in the well of PDA agar plates, these agar plates were then incubated at temperature of 37˚C and zone of inhibition was well measured in mm.

Antioxidant activity by ABTS and DPPH radical scavenging assay. Anti-oxidant are compounds having potential to reduce the effects of free radicals of produced by oxidative stress in body, which is generated in various disease. Co_3O_4 NPs prepared from cow urine and hydrothermally synthesized ZnO NRs are analyzed for their antioxidant potential by performing commonly used ABTS and DPPH methods. ABTS radical scavenging assay was performed as described by Re et al [21] with few modifications [22]. 50 µL of nanomaterials water extract with 1µg/ml of concentration mixed with 2950µL of ABTS reagent. Thereafter, the absorbance of the aliquot was measured after 2 hrs incubation under dark condition and measured at 734 nm to produce a sample. To produce a control, methanol (99.5%) was used as a blank solution and its absorbance was recorded. Positive control was ascorbic acid.

DPPH assay was carried out using the method as described by Brand Williams [23] with slight modification [24]. The reaction was done by mixing 40 µL (1µg/ml) nanomaterials with 3 mL of DPPH reagent and incubation was done by avoiding light oxidation for 30 min. The spectrophotometric absorbance at 517 nm was used to determine the decrease of the DPPH radical. The radical-scavenging activity (RSA) is calculated using the Eq. (1),

$$RSA\left(\%\right)=\frac{\text{A}\text{c}\text{o}\text{n}\text{t}\text{r}\text{o}\text{l} - \text{A}\text{s}\text{a}\text{m}\text{p}\text{l}\text{e}}{\text{A}\text{c}\text{o}\text{n}\text{t}\text{r}\text{o}\text{l}}\times 100 \quad (1)$$

…….

Where, Asample is the absorbance of the solution when the sample has been added at a particular level,

Acontrol is the absorbance of the DPPH or ABTS solution.

In vitro **Assays for Anti-inflammatory study**

Protein denaturation assay. Denaturation of protein cases changes in the physiochemical property of protein which is caused by inflammatory agents this method is explained by Grant et al [25] with slight modification[26]. 50µl working solution of nanomaterials is diluted with 450 µl of 5% w/v BSA then it was incubated for 37°C for 20 minutes and heated at 57°C for 3

minutes. Tubes were cooled under running water and diluted with 2.5 ml phosphate buffer saline and absorbance was measured at 660 nm. Percent of inhibition of the Fetal Bovine Serum (BSA) protein is calculated by the Eq. (2),

$$\text{BSA Denaturation inhibition (\%)} = \frac{\text{Acontrol} - \text{Asample}}{\text{Acontrol}} \times 100 \quad (2)$$

Where; Acontrol is absorbance of the control,

Asample is absorbance of the test sample.

Leukocyte membrane stabilization test. This experiment is depending on hypotonicity-induced haemolysis of human red blood cells (HRBC) and the measurement of Hemoglobin content was measured at 560 nm. Experiment was described by Bhurat et al [27] with the small modification described [28]. Diclofenac (50µg/ml) was used as a standard medicine in this study. Measurements of percent stabilization of Leukocytes (Eq. (3)) by considering control as 100%.

$$\text{RBC Stabilization (\%)} = 100 - \left(\frac{\text{Asample}}{\text{Acontrol}}\right) \times 100 \quad (3)$$

Where, Acontrol is absorbance of the control,

Asample is absorbance of the test sample.

Results And Discussion

XRD study. The poly-dispersed crystalline nano-material is revealed by the XRD spectrum. The XRD patterns of Co_3O_4 NPs, ZnO NRs, and their composites are shown in Fig. 2. The peak position denotes the unit cell's translational symmetry, i.e., its size and shape, whereas the peak intensities denote the electron density within the unit cell. Co_3O_4 NPs show Bragg's reflections, as shown in Fig. 2a, (enlarged spectra on right side) with 2θ values at 31.382, 36.9599, 44.8974, 59.4242, and 65.3031 representing (220), (311), (400), (511), and (440) planes, respectively; these planes are due to the cubic Nano crystalline structure of Co_3O_4 NPs. The pattern was dependable, as evidenced by card No. 01-076-1802 in the JCPDS database [29].

The spectra of ZnO NRs (Fig. 2d) corresponds to JCPDS card No.03-065-3411, confirming the hexagonal wurzite-type structure. The observed 2θ values of ZnO NRs are: 31.8383, 34.4921, 36.3209, 47.5976, 56.6386, 62.8961, 66.4211, 67.9848, 69.1256, 72.6216, 76.992, 81.4166, and 89.631, which correspond to the (h k l) values (100), (002), (101), (102), (110), (103), (200), (112 (203). The JCPDS cards show that the synthesized nanomaterials are entirely crystalline in nature, with no adulterations [30–32]. The spectra of Co 5% and Co 10% (Fig. 2b and c) give the conformation of sythesis of nanomaterials. This spectra corresponds to JCPDS cards 01-076-1802 (Co_3O_4 NPs) and 03-065-3411 (ZnO NRs) (enlarged spectrum on right side).

The Debye–Scherer's formula (Eq. (4)) was used to compute crystallite size of the nanomaterials from the Full Width at Half Maxima (FWHM) denoted by β and Diffraction angle (θ),

$$D = \frac{0.9}{\text{cos}}$$

4

……..

here in Eq. (4) where λ is the wavelngth of x-ray used for diffraction (0.1540 nm).

The crystallite size for various samples are calculated using above formala and represented in Table no. 1 for Co_3O_4 NPs and in Table no. 2 for ZnO NRs.

Morphology Index (MI). The interrelation between particle size and morphology determines the specific surface area of a NPs. FWHM is used to determine MI. MI is calculated using the following Eq. (5),

$$\text{MI}=\frac{\text{FWHM}}{\text{FWHM} + \text{FWHM}}$$

5

……

The particulate FWHM value of a peak is $FWHM_p$, and $FWHM_h$ is the highest FWHM value obtained from peaks.

The MI value of Co_3O_4 NPs ranges from 0.4998 to 0.6667 (Table no.1), whereas the estimated values of ZnO NRs also range from 0.4998 to 0.6667 (Table no.2). It is linked to the size of crystalline particles and the Specific Surface Area (SSA). Co_3O_4 NPs have an SSA value of 2.8543–29.8414 m^2/g (Table no.1), while ZnO NRs have an SSA value of 12.6294–29.5411 m^2/g (Table no.2). According to the estimated data, MI is directly proportional to particle size and inversely proportional to SSA with a minor fluctuation. Figure 3(a-b) and Fig. 4(a-b) show the results. The linear fit indicates the deviations and relationships between the figures.

Surface morphology. FESEM was used to study the shape and size of synthesized nanomaterials and their composites (Fig. 5). Furthermore, looking at the low magnification, it shows that particles grown at a high density are spherical shaped. On further magnification, it reveals that Co_3O_4 NPs tend to agglomerate. Most of the synthesized Co_3O_4 NPs lies in the size range of 100 nm – 400 nm. (Fig. 5.1). Apart from major spherical shape some irregular shaped nanomaterials are observed in FE-SEM imaging [33]. The FESEM image (Fig. 5.2 and 5.3) of the synthesized nanocomposite flashes the formation of Co_3O_4 NPs anchored on the surface of the ZnO NRs. Speculation of the image reveals that the ZnO NRs are well aligned and the Co_3O_4 NPs are randomly dispersed in them. The FESEM images of the NRs are shown in Fig. 5.4 and 5.5. The FESEM image reveals that the diameters of the ZnO NRs lie in the range of 600–1000 nm, and the length of the nano rod is in the range of 2000–3000 nm.[34]. Furthermore, Fig. 5 also shows the elemental mapping of Co_3O_4 NPs, ZnO NRs and their composites. Firstly, in Fig. 5.1 a-c, 5.2 a-d, 5.3 a-d and 5.5 a-c, we can see the combined mapping of elements. Nevertheless, Fig. 5 consists of individual mappings of the elements Cobalt, Oxygen, and Zinc.

Energy Dispersive Spectroscopy (EDS) analysis. Elemental composition analysis of synthesized nanomaterials and their composites have been studied through the Energy Dispersive (ED) spectra. The characteristic ED spectra are shown in Fig. 6 and the analysis results are summarized in table. In the spectrum of Co_3O_4 NPs (Fig. 6a), 4 peaks are observed, which are identified as Cobalt and Oxygen however, in the spectrum of ZnO NRs (Fig. 6d) there are also 4 peaks with Zinc and Oxygen[35]. Even the traces of impurities and other elements are not observed. The observed composition ratios of Co_3O_4 and ZnO in the composite are consistent with expected composition ratio and it is shown in Fig. 6b and Fig. 6c. This indicates that the expected stoichiometry under preparation is well maintained in the samples prepared using the mortar-pestle[36].

In order to explain the composition of material in wt%, in Co_3O_4 NPs, 73.40% out of total weight is cobalt and remaining is oxygen. Moreover, talking about composites in Co 5% and Co 10% the largest portion of total weight is acquired by Zinc i.e. 78.82% and 76.22% respectively. However, the smallest portion is made up of Cobalt contains 2.43% and 4.16% not to mention, remaining is Oxygen out of total weight. ZnO NRs consists 17.48% of Oxygen and 82.52% of Zinc.

FTIR Analysis. FT-IR spectrum of ZnO, Co_3O_4 and ZnO- Co_3O_4 Nano-composites were recorded in the range 4000 cm^{-1} to 400 cm^{-1}. The plot (Fig. 7) illustrates the FT-IR spectrum of the Co_3O_4 NPs, Co 5%, Co 10% nanocomposite and ZnO NRs. Overall, this spectrum gives the information about different types of vibrations in these samples. not to mention, the data of Co_3O_4 NPs shown in Fig. 7a is the fingerprint of Co_3O_4. Shading the light, the spectrum of Co_3O_4 NPs, Co 5%, Co 10% and ZnO NRs, a broad peak centered at 3395, 3498, 3500 and 3390 cm^{-1} is because of δ(H–O – H)[37]. In Fig. 7 (b-c), the Co 5% and Co 10% asymmetric stretching vibration $–CH_3$ and $–CH_2$ groups absorption bands, respectively, were observed at 2922 cm^{-1} and 2923 cm^{-1} while the ZnO stretching vibration of the $–CH_2$ group is at 2810 cm^{-1} and it is illustrated in Fig. 7d. However, -OH groups of water molecules are responsible for a small peak centered at 1629, 1635 and 1623 cm^{-1} in spectrum of all samples except ZnO Nano rods, further next, these peaks show the presence of humidity. Besides these δN-H (amide II) group is confirmed due to presence of significant peak at 1530, 1521 and 1598 cm^{-1}in Co_3O_4, Co 5% and ZnO NRs respectively. In a same way, the transmittance band at 1383, 1385 and 1386 cm^{-1} in Co 5%, Co 10% and ZnO NRs resulted into the presence of group vC-N (amide III) moreover, the band at 1103 cm^{-1} in Co_3O_4 NPs, and 1168 (for Co 5% & 10%) and 1120 cm^{-1} in ZnO NRs occurs because of the stretching vibrations C-C linkages correspondingly[38]. The stretching vibrations of C–O stretching cause the band to appear at 1068 – 1020 cm^{-1} in Co 5%, Co 10% and ZnO. The bands between 900–920 cm^{-1} are due to H-C-N functional group. The peak at 840 cm^{-1} in ZnO shows there is C = C bending. The peak ranges from 780 – 700 cm^{-1} are due to C-H bending, nevertheless, the peak in 700 – 630 cm^{-1} range accounts for $Co^{2+}–O^{2-}$ in tetrahedral coordination and the peak in 630 – 550 cm^{-1} range stands for $Co^{3+}–O^{2-}$ in octahedral coordination[39]. The transmittance peak at 495 cm^{-1} is likewise ascribed to Zn-O vibrations [40].

Raman Spectroscopic Analysis. The optical properties of as synthesized Co_3O_4 NPs, ZnO NRs and their composites were characterized using Raman spectroscopy. The presence of defects was detected using Raman spectroscopy, which was utilized to detect the disorder caused by dopant incorporation in the host lattice. The Fig. 8 illustrates the Raman Spectra of Co_3O_4 NPs, Co 5%, Co 10% Nano composite and ZnO NRs samples taken at RT in the range of 100–3250 cm^{-1}. It is observed that, in Fig. 8a, 8b and 8c there is a common peak at 691 cm^{-1}, which is because A1g phonon mode of Co_3O_4. However, there are two common peaks in Fig. 8b, 8c and 8d at 101 and 436 cm^{-1} respectively [41]. The nonpolar modes (E2) are Raman active and have two frequencies E2 (high) and E2 (low) associated with the vibration of the oxygen atom and vibration of Zn atoms, The peak at 101 cm^{-1} represents the $E2_{(Low)}$ (E_{21}) mode, furthermore the peak at 360 cm^{-1} represent the $E2_{(High)}$ ($E2_h$) mode [42]. The characteristic D and G bands for nanocomposites of Co 5% and Co 10% were D bands observed value is 1347 cm^{-1} and G bands observed value is 1620 cm^{-1}, respectively.

Particle Size Distribution. Dynamic light scattering (DLS) can be used to determine the hydrodynamic diameter of produced nanoparticles, nanorods, and nanocomposites. Figure 9 shows the DLS, which reveals the hydrodynamic diameter of the produced nanomaterials.

When light passes through a colloidal solution, it bombards microscopic particles and scatters in every way possible (i.e. Rayleigh scattering). Even whether the incident light is monochromatic or laser, we see a fluctuation in the intensity of light. This fluctuation in light intensity is caused by Brownian motion in solution, which is constantly occurring. DLS, also known as photon correlation scattering, is a common name for this approach.

The average particle size of biogenic Co_3O_4 NPs (Fig. 9a) was 729 nm, according to DLS. Biogenic Co_3O_4 NPs have a strong peak, indicating mono-dispersed nature. Figure 9d shows the distribution of ZnO NRs by size, which ranges from 1000 to 3000 nm. ZnO NRs have an average particle size of 1733 nm. The poly-dispersed nature of ZnO Nanorods can be seen in their broad size distributions. Figure 9b and Fig. 9c show the particle size distribution of nanocomposites. Ball milling lowers the particle size of both nanocomposites when compared to ZnO NRs. The particle size of Co 5% is 810 nm. Co 10% has a diameter of 1156 nm. Both the Nano composites are poly-dispersed [43].

Electro kinetic Potential and Zeta Potential. To find out the stability of synthesized nanomaterial Electro kinetic Potential was used, additionally, it also shades light on the dispersion stability of colloidal solution and mobility of nanoparticles as well. As the value of zeta potential, either positive or negative are higher, the material is more stable.

The Fig. 10a consist the zeta potential value of the Co_3O_4 NPs however the value is -17.3 mV, Furthermore, looking at the Fig. 10d, ZnO NRs shows the zeta potential value − 30.5 mV. The high negative zeta potential (ξ) value supports long-term stability, good colloidal nature and high dispersity of ZnO NRs due to negative-negative repulsion. Figure 10b and Fig. 10c illustrate the zeta potential value of Co 5% and Co 10% and the values are − 30.0 mV and − 34.6 mV respectively. The synthesized nanomaterials have zeta potential values between − 35 to 0 mV have outstanding stability nevertheless, the dispersion stability also effects on the zeta potential values [44,45].

Thermogravimetric analysis. At a heating rate of 10°C/min, Fig. 11 (a-d) shows typical TGA/DSC curves of biosynthesized Co_3O_4 NPs, ZnO NRs, and their nanocomposites. The TGA profile of Co_3O_4 NPs, which show a larger weight loss than others, shows a steady weight reduction with two quasi-sharp shifts at 463°C and 917°C, followed by a practically constant plateau. The solvent is to blame for the weight loss. The evaporation of water molecules and nitrogen causes a 4.49% weight loss from 100 to 463°C. Nitrogen loss leading to nitrate breakdown causes the peak at 463^oC. However, due to the phase change of the material, there is a weight loss of 15.83% between 463^o C and 1000^oC. [29,46].

When it comes to ZnO NRs, annealing at temperature over 300°C appears to ensure the creation of stable ZnO NRs. The loss of volatile surfactant molecules adsorbed on the surface of Zn complexes during synthesis conditions might account for the weight up to 300^oC. The conversion of Zn complex to Zinc hydroxide is responsible for the exothermic peak about 333°C. The creation of ZnO NRs and the degradation of organic molecules might be attributed to the 2nd exothermic peak at 535°C. A 96.53% residual is left after the last degradation, which takes place at 700°C and produces ZnO with a wurtzite-like structure that is stable up to 1000°C[47]. In short, ZnO NRs were more thermally stable as compared to the Co_3O_4 NPs.

Co 5% and Co 10% shows relevantly similar results, with the two endothermic peaks. The 1st peak is at 200^oC and 181^oC, respectively. These peaks are due to the different weight variation of the Co_3O_4 NPs and ZnO NRs. Moreover, the peak at 353 ^oC and 359 ^oC discretely, were present because of the conversion of the zinc hydroxide into zinc oxide. At last, both of the samples leave the 95.36% and 95.22% of residue [48].

Determination of antimicrobial Activities of ZnO NRs, Co_3O_4 NPs and nanocomposite (Co 5% and Co 10%). The minimum inhibitory concentrations (MIC) of Co_3O_4 NPs, ZnO NRs and there nanocomposites were studied by turbidity measurement using spectrophotometric method at 625 nm [49]. At lower concentrations of 50 to 200 g/mL, zero growth was detected under a spectrophotometer, indicating that this concentration has strong bactericidal action, which is essential in the manufacture of antibacterial compounds. The existence or absence of turbidity, which was evaluated by + or – in table no. 3, was demonstrated. Because of bacterial growth, lower concentrations of nanomaterials appear turbid. This suggests that NPs at lower concentrations have minimal antibacterial effect. Result also concludes that combination of 90% ZnO + 10% Co_3O_4 shows good potential bactericidal activity among all nanomaterials samples. The results also showed that bacterial strains like *Staphylococcus aureus* and *Salmonella typhi* were extremely susceptible to nanomaterials, but *Bacillus cereus* and *Escherichia coli* had reduced bactericidal efficacy as seen by observable growth. Previous study by raj et al demonstrated MIC of zinc nanoparticle prepared from *Brassica oleraceae* leaves against similar type of bacteria[50] .

Earlier report on different methodology for nanoparticle preparation and application from cow urine were detailed discussed by Dabhane et al [51]. Previous literature on structural properties of ZnO NRs and antibacterial proficiency of based on four mechanisms for the production of reactive oxygen species (ROS) were studied by Bruna Lallo da Silva et al in-review study [14] which is similar relation with current study.

These antibacterial and antifungal strategies for nanomaterials prepared were assessed against a set of four bacterial and two fungi strains shown in table no. 4. The presence or absence of inhibition zones in mm was used to measure potency

qualitatively. The observations are represented in table no. 4 indicates that, the concentrations of 200 µg/mL nanomaterials extract are showing higher significant antimicrobial activity against all gram-negative bacterial strains and are depicted in tabular form in table no. 4. The zone of inhibition observed is 17 ± 0.81 mm for microbe *S. aureus* which conclude to be better activity similar ZnO NRs using solanum nigrum leaf extract in both Gram positive (*S. aureus*) and Gram negative (*S. paratyphi,V. cholerae, E. coli*) bacteria were studied by Ramesh et al [52]. In *A. niger* the minor antimicrobial spectrum of inhibition zone was found (15.66 ± 0.94) than *Fusarium solani (*14.66 ± 0.47*)* which indicate highest antifungal activity in Co 5% sample. A result clearly shows that, the combination method has more advantages compared with some other singular metallic cow urine nanoparticle preparation methods.

Antioxidant Activity. Antioxidants are free radical molecules that are created by a variety of systems that have the potential to harm biological cellular processes. ABTS and DPPH are two methods that are often used for measuring free radical destructive activity [53]. The DPPH and ABTS scavenging activities of nanomaterials are shown in Fig. 12 in comparison to standard antioxidant ascorbic acid, indicating maximum antioxidant activity, whereas the cumulative effect of Co_3O_4 NPs shows maximum potential, which is 42.41 ± 0.18% in DPPH radical savaging activity and 42.41 ± 0.18% in ABTS radical scavenging activity at 100µg/ml, whereas standard ascorbic acid shows 75.68 ± 0.47% activity.

The dark violet color of the DPPH was gradually decreasing over a time interval and a decrease in absorbance was also recorded. The decrease in the absorption intensity confirms the good scavenging activities of DPPH; this is due to its capability of good oxidant, electron loosing and capping agent present on the surface of different nanomaterials. Our results are similar contact with Ag_2O and ZnO NRs using cow urine have different application in photoluminescence, photolytic, antibacterial and antioxidant activities are reported previously by Vinay et al [54] and Dabhane et al [51]. Significantly, the biogenic synthesis of Co_3O_4 NPs and the hydrothermal synthesis of ZnO NRs exhibit a broad spectrum of antibacterial and antioxidant activity. As a result, it signifies promising antioxidants and antibacterial agents with potential use in the synthesis of pharmaceutical drugs. The order of maximum DPPH potential and ABTS potential is Co 10% ▯ Co 5% ▯ ZnO NRs ▯ Co_3O_4 NPs and Co 5% ▯ZnO NRs ▯ Co 10% ▯ Co_3O_4 NPs respectively. The order of value is 42.41 ± 0.18 ▯ 40.57 ± 0.58 ▯ 39.88 ± 0.43 ▯ 34.88 ± 0.48 and 36.19 ± 0.25 ▯ 34.97 ± 0.28 ▯ 29.89 ± 0.35 ▯ 26.66 ± 0.47.

Anti-inflammatory study. Previous literature by Agarwal et al clearly determines the mechanism-based anti-inflammatory properties of the NPs from several metal and metal oxide [55]. NPs having promising anti-inflammatory properties due to their large surface area to volume ratio, which will be better at blocking inflammation enhancer's e.g cytokines and inflammation-assisting enzymes. The *in vitro* assessment of BSA denaturation potential which results in anti-inflammatory effects of nanoparticles assessed against heat induced egg albumin denaturation are summarized in Fig. 13. In a concentration-dependent manner, all tested doses effectively inhibited the denaturation of egg albumin. Whereas the max. BSA Denaturation % inhibition was 73.53 ± 0.14% observed at the concentration of 200µg/mL (highest) of Co 10%. The order of maximum was show below is Co 10% ▯ Co 5% ▯ ZnO NRs ▯ Co_3O_4 NPs and values are 67.46% ▯ 63.03% ▯ 66.40% ▯ 59.04%. While aspirin, used as standard drug exhibited an inhibition of 61.91 ± 0.24% at the concentration of 50 µg/mL.

RBC Stabilization of Leukocyte is one of the methods used to measure inflammatory response by measuring the hemoglobin absorbance spectrophotometrically at 560 nm. Anti-inflammatory drug possibly lyses and usually makes the reorganization of lymphocytes, that results in fast reduction in the peripheral blood lymphocyte number which cases longer term response. Because the erythrocyte membrane is comparable to the lysosomal membrane, the HRBC technique was chosen for in vitro assessment of anti-inflammatory efficacy. Its stabilization means that the NPs may just as well stabilize lysosomal membranes. Results demonstrated in Fig. 13 indicate that water extract of Co 10% solution shave noteworthy anti-inflammatory action at various concentrations. Whereas of ZnO NRs and Co_3O_4 NPs separately gives lower RBC Stabilization of Leukocyte (%) which is 15.15 ± 0.24% and 13.65 ± 0.24% Respectively at concentration of 200 µg/mL. Where, Co 5% showed small lower anti-inflammatory potential when compared with the Co 10% and standard drug diclofenac have potential 27.52 ± 0.94% which is shown in Fig. 13. The given results are similar to previous literature of anti-inflammatory potential and

antioxidant of zinc oxide nanoparticles synthesized using Polygala tenuifolia root extract [56] further study of anti-inflammatory and antinociceptive activities in the mice model were explained by liu et al [57].

Conclusions. The results confirm that the biomolecules present in the physiologically processed liquid metabolic waste of Indian cows are responsible for the successful formation of cobalt oxide nanomaterials. When we analyze these materials, we discover that they have unique characterization results. We have the composite's conformation by XRD spectra and EDX analysis. Because of the low zeta potential value, the morphology of Co_3O_4 NPs is aggregation form as compared to others. This suggests that the substance isn't very stable. But the stability is increased by making a composite of ZnO and Co_3O_4. In FTIR, we observed that both Co^{2+} and Co^{3+} species are present in our material, as well as the conformation of the Zn-O bond. The results demonstrated an expensive, straight forward, and eco-friendly method for synthesizing Co_3O_4 NPs, ZnO NRs, and their composites, which verified excellent antioxidant, antimicrobial, and anti-inflammatory activities. Thus, we believe that all of this new nanomaterial should be considered as a possible drug for management and treatment of various disorders. Furthermore, it was determined that the combination of ZnO NRs and Co_3O_4 NPs (10% Co + 90% ZnO, 5% Co + 95% ZnO) has greater in vitro anti-inflammatory and antioxidant potential than single ZnO NRs and Co_3O_4 NPs.

Declarations

Data availability

The data presented in this study are available on request from the corresponding author.

Acknowledgements

The authors are thankful to Miss. Aasiya Jamadar for possible help during the progress of research work. Mr. Suresh Suryawanshi sincerely thanks to Indian Council of Medical Research (ICMR) for providing SRF fellowship [Award No. 45/6/2019/MP/BMS].

Author information

Authors and Affiliations

School of Nanoscience and Technology, Shivaji University, Kolhapur-416004 (MH), India.

Omkar S. Karvekar, Apurva S. Vadanagekar, Prashant D. Sarvalkar, Sarita M. Jadhav, Richa D. Singhan, Kiran Kumar K Sharma and Neeraj R. Prasad.

Department of Biochemistry, Shivaji University, Kolhapur-416004 (MH), India.

Suresh S. Suryawanshi and Jyoti P. Jadhav.

Contributions

Conceptualization, O.S.K., A.S.V, P.D.S. and N.R.P.; methodology, O.S.K., A.S.V. and P.D.S.; formal analysis, O.S.K., A.S.V., R.D.S., and S.M.J.; resources, J.P.J and K.K.S.; investigation, P.D.S. , S.S.S.; writing, O.S.K., A.S.V., review, P.D.S. and N.R.P. All authors have read and agreed to the published version of the manuscript.

Corresponding authors

Correspondence to Neeraj R. Prasad.

Ethics declarations

Competing interests

The authors declare no competing interests.

References

1. Li, H. *et al.* Electrochimica Acta Zinc cobalt sul fi de nanoparticles as high performance electrode material for asymmetric supercapacitor. *Electrochim. Acta* **319**, 716–726 (2019).
2. Rasheed, T. *et al.* Carbon nanotubes-based cues : A pathway to future sensing and detection of hazardous pollutants. *J. Mol. Liq. J.* **292**, (2019).
3. Karvekar, O. S., Sarvalkar, P. D., Vadanagekar, A. S., Singhan, R. D. & Jadhav, S. M. Biogenic synthesis of silver anchored ZnO nanorods as nano catalyst for organic transformation reactions and dye degradation. *Appl. Nanosci.* (2022) doi:10.1007/s13204-022-02470-1.
4. Patil, A. A. *et al.* Bipolar-resistive switching and memristive properties of solution- processable cobalt oxide nanoparticles. *J. Mater. Sci. Mater. Electron.* (2020) doi:10.1007/s10854-020-03515-3.
5. Wang, X. *et al.* Construction of cobalt nanoparticles decorated intertwined N-doped carbon nanotube clusters with dual active sites for highly effective 4-nitrophenol reduction. *J. Alloys Compd.* **858**, 158287 (2021).
6. Sarvalkar, P. D. *et al.* Bio-mimetic synthesis of catalytically active nano-silver using Bos taurus (A-2) urine. *Sci. Rep.* **11**, 1–17 (2021).
7. Waris, A. *et al.* Green fabrication of Co and Co 3 O 4 nanoparticles and their biomedical applications : A review. *Open Life Sci.* **16**, 14–30 (2021).
8. Khezri, K., Saeedi, M. & Maleki, S. Biomedicine & Pharmacotherapy Application of nanoparticles in percutaneous delivery of active ingredients in cosmetic preparations. *Biomed. Pharmacother.* **106**, 1499–1505 (2018).
9. Sarvalkar, P. D. *et al.* A review on multifunctional nanotechnological aspects in modern textile. *J. Text. Inst.* **0**, 1–18 (2022).
10. Prasad, R. D. *et al.* A Review on Concept of Nanotechnology in Veterinary Medicine. *ES Food Agrofor.* 28–60 (2021) doi:10.30919/esfaf481.
11. Jadoun, S., Arif, R., Jangid, N. K. & Meena, R. K. Green synthesis of nanoparticles using plant extracts: a review. *Environ. Chem. Lett.* **19**, 355–374 (2021).
12. Bajaj, K. K., Chavhan, V., Raut, N. A. & Gurav, S. Journal of Ayurveda and Integrative Medicine Panchgavya : A precious gift to humankind. *J. Ayurveda Integr. Med.* **13**, 100525 (2022).
13. Meena, M. *et al.* Go mutra (Cow urine) and its uses : An overview. *J. Entomol. Zool. Stud.* **7**, 1218–1222 (2019).
14. Nazeruddin, G. M. *et al.* Bos taurus Urine Assisted Synthesis of Cadmium Nanoparticles. *DER PHARMA Chem.* **9**, 39–43 (2017).
15. Padvi, S. R. P. M. N., Shaikh, S. S. S. Y. I., Samant, L. S. C. A. P. & Prasad, N. R. Bio - inspired synthesis of catalytically and biologically active palladium nanoparticles using Bos taurus urine. *SN Appl. Sci.* **2**, 1–12 (2020).
16. Antimicrobial, P. & Therapy, A. Bos taurus Urine Assisted Biosynthesis of CuO Nanomaterials : A New Bos taurus Urine Assisted Biosynthesis of CuO Nanomaterials : A New Paradigm of Antimicrobial and Antineoplatic Therapy. *Macromol. Symp.* **392**, 1900172 (2020).
17. Dabhane, H. *et al.* Cow urine mediated green synthesis of nanomaterial and their applications: A state-of-the-art review. *J. Water Environ. Nanotechnol.* **6**, 81–91 (2021).
18. Dastager, S. G., Sreedhar, B., Dayanand, A. & Shirley. Antimicrobial Activity of Silver Nanoparticles Synthesized from Novel Streptomyces Species. *Dig. J. Nanomater. Biostructures* **5**, 447–451 (2010).
19. Suryawanshi and Rane, M. R. S. Antioxidant , Antimicrobial Activity with Mineral Composition and LCMS Based Phytochemical Evaluation of Some Mucuna Species from India. *Int. J. Pharm. Biol. Sci.* **9**, 312–324 (2019).
20. Kamble, P., Suryawanshi, S., Jadhav, J. P. & Attar, Y. C. Enhanced inulinase production by Fusarium solani JALPK from invasive weed using response surface methodology. *J. Microbiol. Methods* **159**, 99–111 (2019).

21. Re, R. *et al.* Antioxidant activity applying an improved ABTS radical. *Free Radic. Biol. Med.* **26**, 1231–1237 (1999).
22. Suryawanshi and Rane. Antioxidant , Antimicrobial Activity with Mineral Composition and LCMS Based Phytochemical Evaluation of Some Mucuna Species from India. *Int. J. Pharm. Biol. Sci.* **9**, 312–324 (2019).
23. Brand-Williams, W., Cuvelier, M. E. & Berset, C. Use of a Free Radical Method to Evaluate Antioxidant Activity. *LWT Food Sci. Technol.* **30**, 25–30 (1995).
24. Suryawanshi, S., Kshirsagar, P., Kamble, P., Bapat, V. & Jadhav, J. Systematic enhancement of L-DOPA and Secondary metabolites from Mucuna imbricata: Implication of precursors and elicitors in Callus culture. *South African J. Bot.* **144**, 419–429 (2022).
25. Grant, N. H., Alburn, H. E. & Kryzanauskas, C. Stabilization of serum albumin by anti-inflammatory drugs. *Biochem. Pharmacol.* **19**, 715–722 (1970).
26. Rane and Suryawanshi. Exploring the proximate composition, antioxidant, anti-Parkinson's and anti-inflammatory potential of two neglected and underutilized Mucuna species from India. *South African J. Bot.* **124**, 304–310 (2019).
27. Bhurat, M., More, S., Sanghavi, R., Salunkhe, P. & Umarkar, A. Preclinical Evaluation of Remusatia Vivipara Leaves Extracts On Haloperidol Induced Catalepsy In Experimental Animals. **1**, (2011).
28. Aware, C. *et al.* Evaluation of L-dopa, proximate composition with in vitro anti-inflammatory and antioxidant activity of Mucuna macrocarpa beans: A future drug for Parkinson treatment. *Asian Pac. J. Trop. Biomed.* **7**, 1097–1106 (2017).
29. Akhlaghi, N., Najafpour-darzi, G. & Younesi, H. Facile and green synthesis of cobalt oxide nanoparticles using ethanolic extract of Trigonella foenumgraceum (Fenugreek) leaves. *Adv. Powder Technol.* **31**, 3562–3569 (2020).
30. Suryavanshi, R. D. *et al. Nanocrystalline immobilised ZnO photocatalyst for degradation of benzoic acid and methyl blue dye*. *Materials Research Bulletin* vol. 101 (Elsevier Ltd, 2018).
31. Theivasanthi, T. & Alagar, M. Titanium dioxide (TiO2) Nanoparticles XRD Analyses: An Insight. (2013) doi:(http://arxiv.org/abs/1307.1091).
32. Huang, N. *et al.* One-step pyrolytic synthesis of ZnO nanorods with enhanced photocatalytic activity and high photostability under visible light and UV light irradiation. *J. Alloys Compd.* (2015) doi:10.1016/j.jallcom.2015.07.039.
33. Kumar, R. *et al.* Spindle-like Co 3 O 4 -ZnO Nanocomposites Scaffold for Hydrazine Sensing and Photocatalytic Degradation of Rhodamine B Dye. 288–300 (2021).
34. Bhat, D. K. Facile synthesis of ZnO nanorods by microwave irradiation of zinc-hydrazine hydrate complex. *Nanoscale Res. Lett.* **3**, 31–35 (2008).
35. Yi, S. H., Choi, S. K., Jang, J. M., Kim, J. A. & Jung, W. G. Low-temperature growth of ZnO nanorods by chemical bath deposition. *J. Colloid Interface Sci.* **313**, 705–710 (2007).
36. Deepty, M. *et al.* XRD, EDX, FTIR and ESR spectroscopic studies of co-precipitated Mn–substituted Zn–ferrite nanoparticles. *Ceram. Int.* **45**, 8037–8044 (2019).
37. Hassanpour, M., Safardoust-hojaghan, H. & Salavati-niasari, M. Degradation of methylene blue and Rhodamine B as water pollutants via green synthesized Co3O4/ZnO nanocomposite. *J. Mol. Liq.* (2016) doi:10.1016/j.molliq.2016.12.090.
38. Cruz, J. C. *et al.* Synthesis and characterization of cobalt nanoparticles for application in the removal of textile dye. *J. Environ. Manage.* **242**, 220–228 (2019).
39. Abdallah, A. M. & Awad, R. Physica B : Physics of Condensed Matter Sm and Er partial alternatives of Co in Co 3 O 4 nanoparticles : Probing the physical properties. *Phys. B Phys. Condens. Matter* **608**, 412898 (2021).
40. Beura, R., Pachaiappan, R. & Paramasivam, T. Photocatalytic degradation studies of organic dyes over novel Ag-loaded ZnO-graphene hybrid nanocomposites. *J. Phys. Chem. Solids* **148**, 109689 (2021).
41. Phan, T. *et al.* Enhancement of multiple-phonon resonant Raman scattering in Co-doped ZnO nanorods Enhancement of multiple-phonon resonant Raman scattering in Co-doped ZnO nanorods. **082110**, (2012).
42. Had, B. *et al.* Journal of Physics and Chemistry of Solids Laser power in fl uence on Raman spectra of ZnO (Co) nanoparticles. **91**, 80–85 (2016).

43. Fan, L. *et al.* Hydrothermal synthesis and photoluminescent properties of ZnO nanorods. *J. Lumin.* **122–123**, 819–821 (2007).
44. Tang, L. *et al.* Cobalt nanoparticles-embedded magnetic ordered mesoporous carbon for highly effective adsorption of rhodamine B. *Appl. Surf. Sci.* **314**, 746–753 (2014).
45. Marsalek, R. Particle Size and Zeta Potential of ZnO. *APCBEE Procedia* **9**, 13–17 (2014).
46. Nouroozi, F. & Farzaneh, F. Synthesis and Characterization of Brush-Like ZnO Nanorods using Albumen as Biotemplate. *J. Braz. Chem. Soc.* **22**, 484–488 (2011).
47. Zhou, N. *et al.* Synthesis and characterization of Zn 1-x Co x O green pigments with low content cobalt oxide. *J. Alloys Compd.* **711**, 406–413 (2017).
48. Xu, C., Wang, X., Zhu, J., Yang, X. & Lu, L. Deposition of Co 3 O 4 nanoparticles onto exfoliated graphite oxide sheets †. 2–6 (2008) doi:10.1039/b809712g.
49. Pfaller, M. A., Messer, S. A. & Coffmann, S. Comparison of visual and spectrophotometric methods of MIC endpoint determinations by using broth microdilution methods to test five antifungal agents, including the new triazole D0870. *J. Clin. Microbiol.* **33**, 1094–1097 (1995).
50. Raj, A., Lawrence, R. S., Jalees, M. & Lawrence, K. ANTI-BACTERIAL ACTIVITY OF ZINC OXIDE NANOPARTICLES PREPARED FROM BRASSICA OLERACEAE LEAVES EXTRACT. *Int. J. Adv. Res.* **3**, 322–328 (2015).
51. Dabhane, H., Zate, M., Bharsat, R., Jadhav, G. & Medhane, V. A novel bio-fabrication of ZnO nanoparticles using cow urine and study of their photocatalytic, antibacterial and antioxidant activities. *Inorg. Chem. Commun.* **134**, 108984 (2021).
52. Ramesh, M., Anbuvannan, M. & Viruthagiri, G. Green synthesis of ZnO nanoparticles using Solanum nigrum leaf extract and their antibacterial activity. *Spectrochim. Acta - Part A Mol. Biomol. Spectrosc.* **136**, 864–870 (2015).
53. Bartkowiak, A. & Roy, S. Alginate Biofunctional Films Modified with Melanin from Watermelon Seeds and Zinc Oxide / Silver Nanoparticles. *Materials (Basel).* **15**, 2381 (2022).
54. Vinay, S. P., Udayabhanu, Nagaraju, G., Chandrappa, C. P. & Chandrasekhar, N. Novel Gomutra (cow urine) mediated synthesis of silver oxide nanoparticles and their enhanced photocatalytic, photoluminescence and antibacterial studies. *J. Sci. Adv. Mater. Devices* **4**, 392–399 (2019).
55. Agarwal, H., Nakara, A. & Shanmugam, V. K. Anti-inflammatory mechanism of various metal and metal oxide nanoparticles synthesized using plant extracts: A review. *Biomed. Pharmacother.* **109**, 2561–2572 (2019).
56. Nagajyothi, P. C. *et al.* Antioxidant and anti-inflammatory activities of zinc oxide nanoparticles synthesized using Polygala tenuifolia root extract. *Journal of Photochemistry and Photobiology B: Biology* vol. 146 10–17 (2015).
57. Liu, H. *et al.* Zinc oxide nanoparticles synthesised from the Vernonia amygdalina shows the anti-inflammatory and antinociceptive activities in the mice model. *Artif. Cells, Nanomedicine Biotechnol.* **48**, 1068–1078 (2020).

Tables

Table no. 1: XRD Analysis and Calculation of Various Parameters for Co_3O_4 NPs

Sr. No.	Peak Position :2θ (degree)	Full width half maxima (Degree)	Full width half maxima (radians)	Particle Size D(nm)	d-spacing (A^0)	For Ag unit cell edges: a=b=c (A^0)	Specific surface area (m^2/g)	Morpho-logical indexing
1	31.382	0.121	0.002111	68.2337	2.85058	8.0720	14.51041	0.666743
2	36.9599	0.1614	0.002816	51.9254	2.43219		20.41525	0.599983
3	44.8974	0.2421	0.004223	35.5234	2.01892		29.84148	0.499982
4	59.4242	0.1614	0.002816	371.388	1.55543		2.854346	0.599983
5	65.3031	0.1476	0.002575	63.9629	1.42773		16.5732	0.62123

Table no. 2: XRD Analysis and Calculation of Various Parameters for ZnO NRs

Sr.No.	Peak Position :2θ (degree)	Full width half maxima (Degree)	Full width half maxima (radians)	Particle Size D(nm)	d-spacing (A^0)	For Ag unit cell edges: a = b ≠c (A^0)	Specific surface area (m^2/g)	Morpho-logical indexing
1	31.8383	0.2017	0.003519	40.98028	2.81076	a = b = 3.2495 c = 5.2069	25.86782	0.545498
2	34.4921	0.2017	0.003519	41.26349	2.60034		25.69028	0.545498
3	36.3209	0.1614	0.002816	51.83253	2.4735		20.45184	0.599983
4	47.5976	0.2421	0.004223	35.8845	1.9105		29.54119	0.499982
5	56.6386	0.2017	0.003519	44.76501	1.62513		23.68079	0.545498
6	62.8961	0.2017	0.003519	46.19228	1.47767		22.94909	0.545498
7	66.4211	0.1614	0.002816	58.86456	1.40755		18.00864	0.599983
8	67.9848	0.1614	0.002816	59.39704	1.37893		17.8472	0.599983
9	69.1256	0.1614	0.002816	59.80096	1.35894		17.72665	0.599983
10	72.6216	0.1614	0.002816	61.11453	1.3019		17.34564	0.599983
11	76.992	0.121	0.002111	83.93634	1.23853		12.62946	0.666743
12	81.4166	0.1614	0.002816	64.96845	1.18204		16.3167	0.599983
13	89.631	0.1614	0.002816	69.42914	1.0938		15.26838	0.599983

Table no. 3: Tabular representation of bacterial growth observed in different concentrations of ZnO NRs, Co_3O_4 NPs, Co 10% and Co 5% nanocomposite after 24 hours

Positive (+): Turbidity in medium due to growth of microbes, Negative (-): Turbidity not occurred in the medium due to no growth. NA- Not contain any sample.

Sample Name/ Strain name	*Conc* µg/mL	*Escherichia coli (NCIM 2662)*	*Salmonella typhi (NCIM 5278)*	*Bacillus cereus* (*NCIM 2217)*	*Staphylococcus aureus (NCIM 5276)*
ZnO NRs	25	+	+	+	+
	50	+	-	+	-
	100	-	-	-	-
	150	-	-	-	-
	200	-	-	-	-
Co_3O_4 NPs	25	+	+	+	+
	50	+	-	+	-
	100	-	-	-	-
	150	-	-	-	-
	200	-	-	-	-
Co 10%	25	+	-	+	+
	50	+	-	+	-
	100	-	-	-	-
	150	-	-	-	-
	200	-	-	-	-
Co 5%	25	+	-	+	+
	50	-	-	-	-
	100	-	-	-	-
	150	-	-	-	-
	200	-	-	-	-
Streptomycin	50	-	-	-	-
Negative Control	NA	+	+	+	+

Table no. 4: Anti-bacterial and Anti-fungal effect exhibited by ZnO NRs, Co_3O_4 NPs, Co 10% and Co 5% nanocomposite on various test microbes.

		Bacterial strains				Fungal stains	
Sample Name/ Strain name	*Conc* µg/mL	*Escherichia coli*	*Salmonella typhi*	*Bacillus cereus*	*Staphylococcus aureus*	*Aspergillus niger*	*Fusarium solani*
ZnO NRs	50	11.33±0.47	12.66±0.94	13.33±0.47	12.66±0.94	12±0.81	10.33±0.47
	100	11.66±0.47	14.66±0.47	13.66±0.47	13.33±0.47	12.33±1.24	11.66±0.94
	150	14.33±0.47	15.00±0	15.33±0.47	15.33±0.47	12.66±0.47	12±0.81
	200	15.66±0.47	16.66±0.47	15.01±0	16.33±0.47	14.33±0.97	13.66±0.47
Co_3O_4 NPs	50	10.33±0.47	12.33±0.47	13.07±0.81	12.0±0.81	12±0.81	11.33±0.47
	100	13±0	14.66±0.47	13.33±0.47	12.33±0.47	12.33±0.47	12±0
	150	12.66±0.47	15.33±0.47	13.33±0.47	13.33±0.47	13±0.81	12.66±0.47
	200	14.66±0.47	15.66±0.47	14±0.81	14.33±0.47	13.66±0.47	13.33±0.47
Co 10%	50	11.66±0.47	13.33±0.47	14±0.81	14.66±0.47	13.33±0.47	11.66±0.47
	100	12.66±0.47	14.33±0.47	15±0.81	15.66±0.47	14.33±0.47	12.33±0.47
	150	15±0	15.33±0.47	15.33±0.47	15.33±0.47	15±0.81	13.66±0.47
	200	16.33±0.47	16.33±0.47	16.33±0.47	17±0.81	15.66±0.94	14.66±0.47
Co 5%	50	11.66±0.94	12.66±0.47	14±0.81	12.66±0.47	11.66±0.47	11.66±0.47
	100	12.66±0.47	13.33±0.47	15.66±0.47	14.66±0.47	13±0.81	11.33±0.47
	150	14.33±0.47	14.33±0.47	14.66±0.94	15.66±0.47	13±0.81	12.33±0.47
	200	15.33±0.47	15.33±0.81	16±0.81	16.66±0.94	14.66±0.47	12.66±0.47
Streptomycin	50	17.66±0.47	17±0.81	17±0.81	18.66±0.47	15.33±0.47	15.66±0.47

Figures

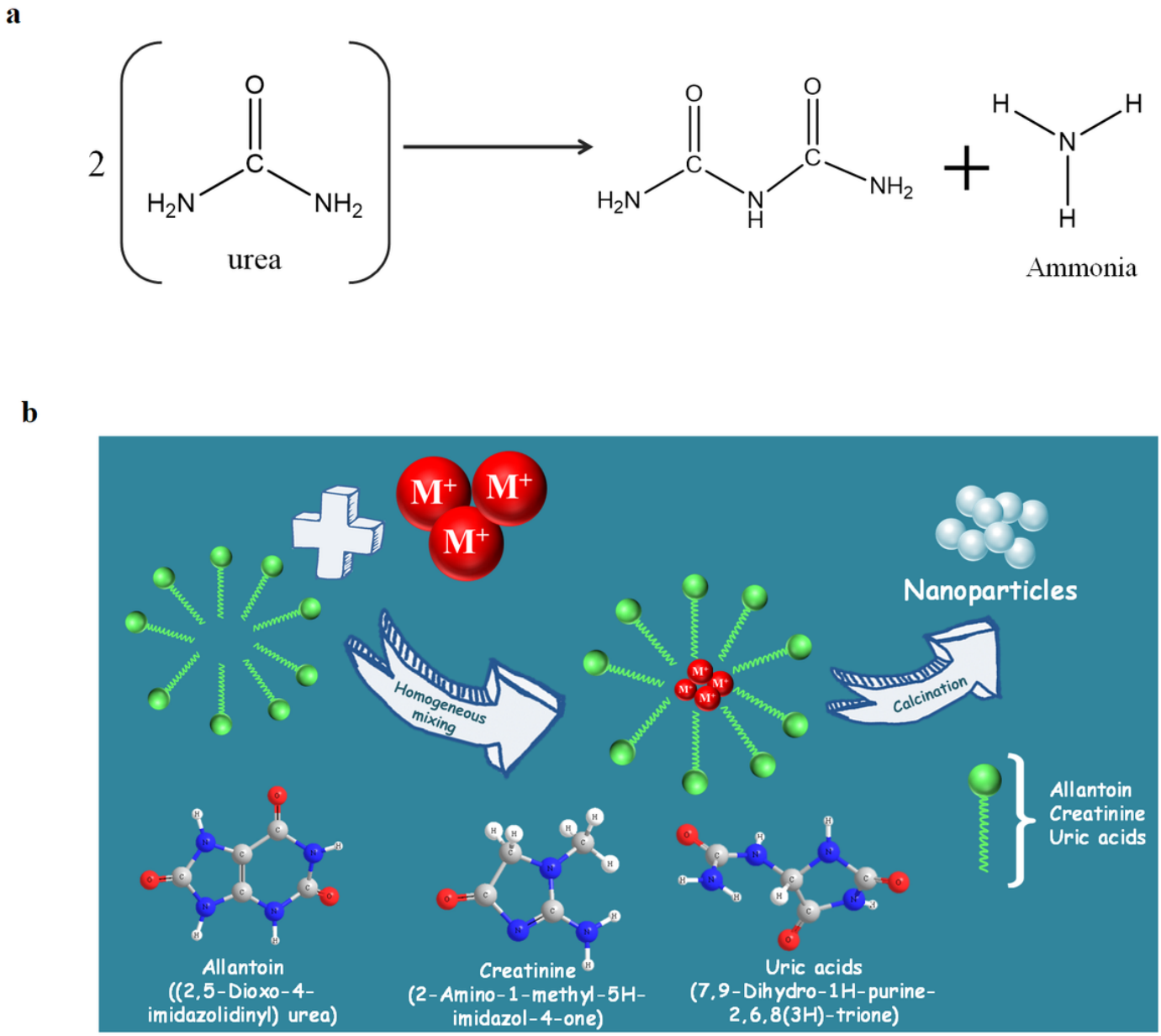

Figure 1

a: Possible mechanism of urea is converted to ammonia through hydrolysis.

b: Probable mechanism of green synthesis of cobalt oxide NPs using Indian cow urine (Redrawn from Ref. [17])

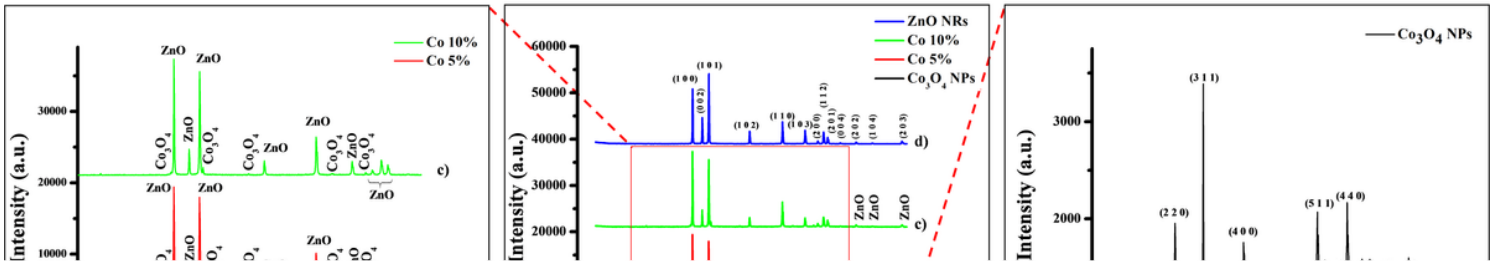

Figure 2

XRD Pattern of (a) Co_3O_4 NPs (b) Co 5% nanocomposite (c) Co 10% nanocomposite (d) ZnO NRs.

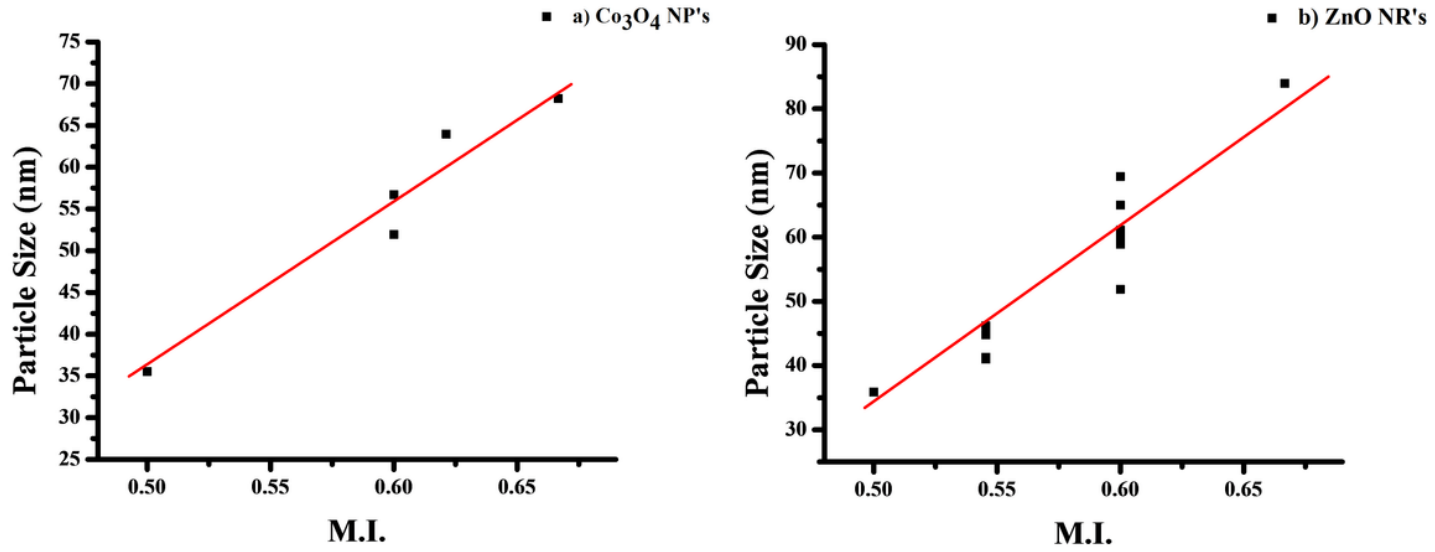

Figure 3

Morphological Index Vs Particle Size of (a) Co_3O_4 NPs (b) ZnO NRs.

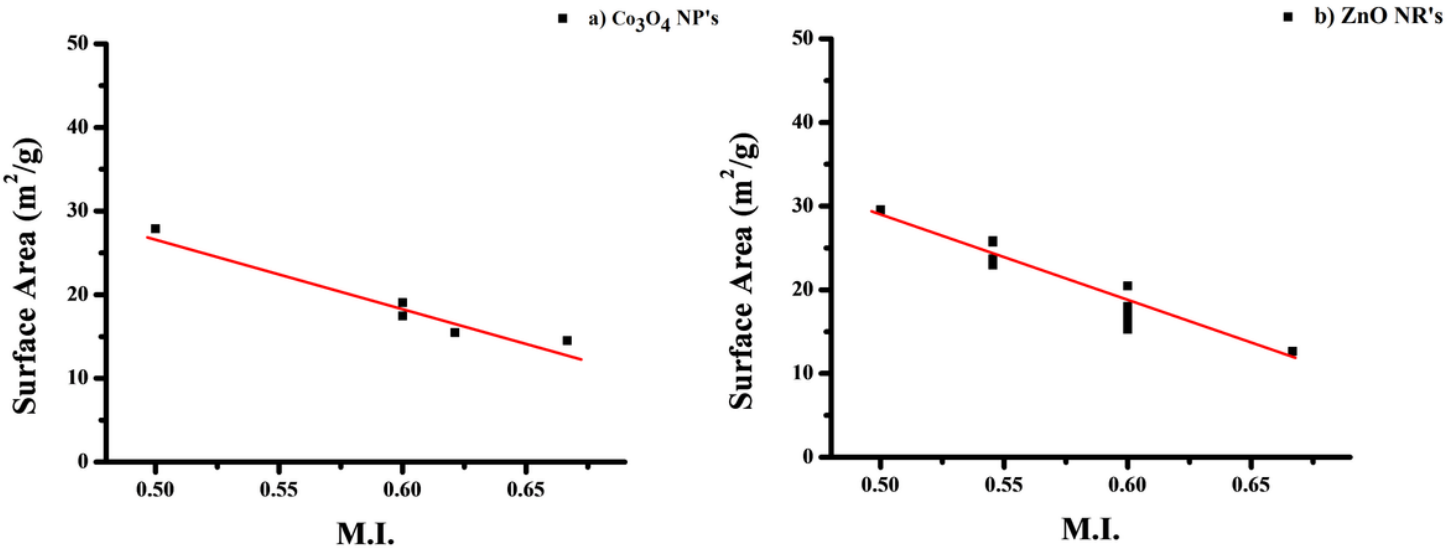

Figure 4

Morphological Index Vs Specific Surface Area of (a) Co_3O_4 NPs (b) ZnO NRs.

Figure 5

FE-SEM analysis of (5.1) Co_3O_4 NPs (5.2) Co 5% (5.3) Co 10% (5.4) ZnO NRs (5.5) ZnO NRs. Elemental Mapping of (5.1a) Co_3O_4 NPs,(5.1b) Oxygen Map, (5.1c) Cobalt Map (5.2a) Co 5%, (5.2b) Zinc Map, (5.2c) Oxygen Map, (5.2d) Cobalt Map, (5.3a) Co 10% (5.3b) Zinc Map, (5.3c) Oxygen Map, (5.3d) Cobalt Map, (5.5a) ZnO NRs(5.5b) Zinc Map, (5.5c) Oxygen Map

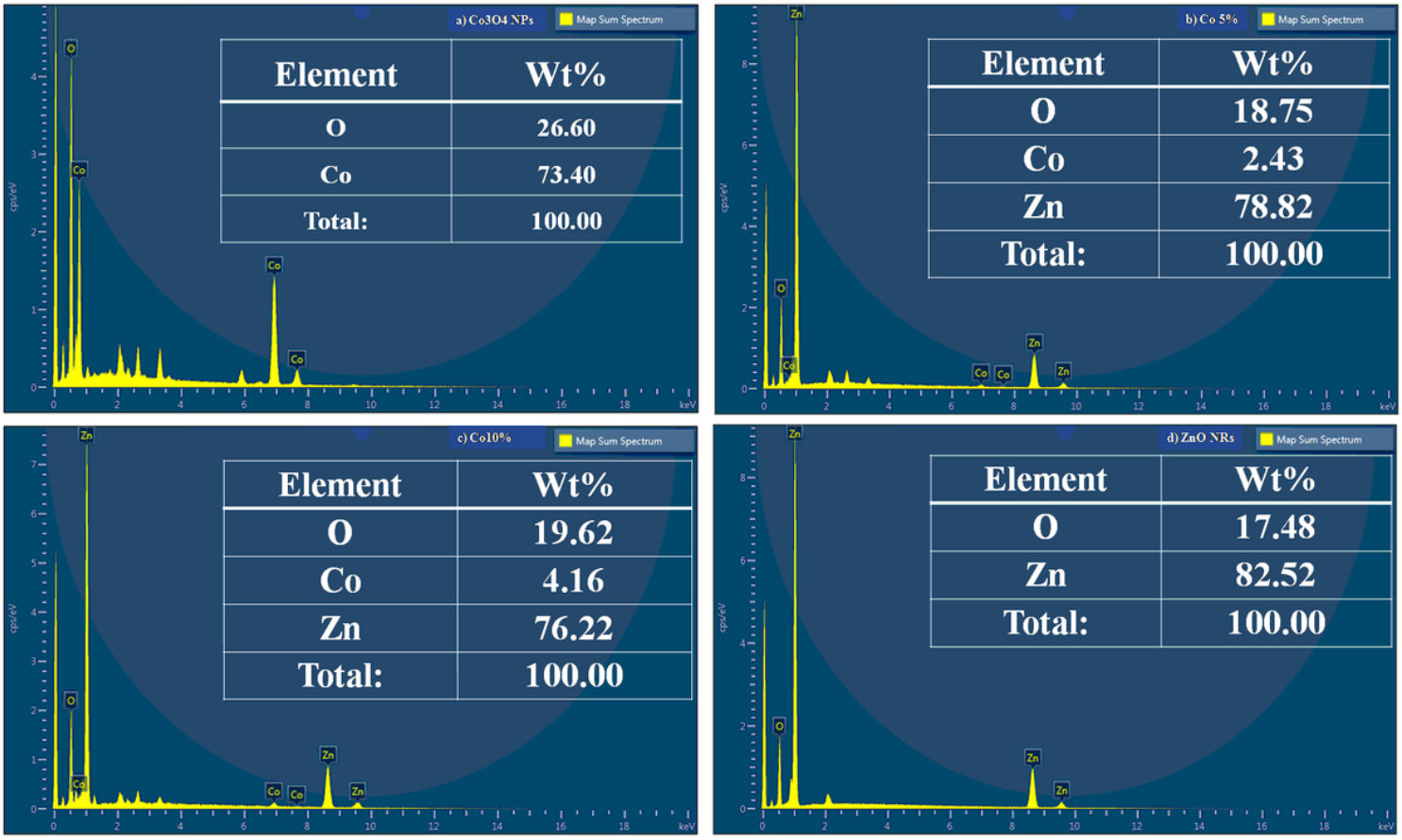

Figure 6

EDS analysis of (a) Co_3O_4 NPs (b) Co 5% nanocomposite (c) Co 10% nanocomposite (d) ZnO NRs.

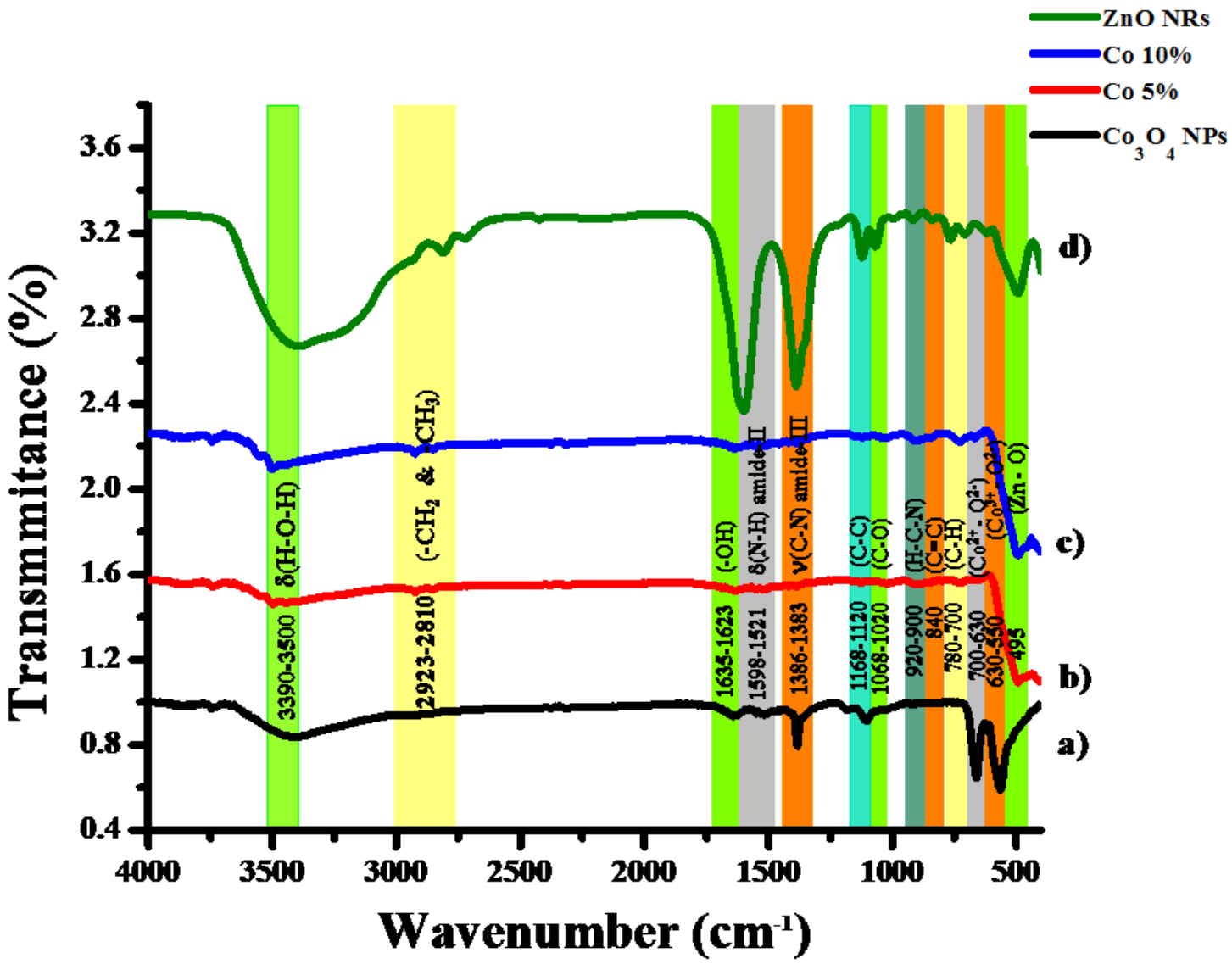

Figure 7

FTIR spectra of (a) Co_3O_4 NPs (b) Co 5% (c) Co 10% (d) ZnO NRs.

Figure 8

Raman spectra of (a) Co_3O_4 NPs (b) Co 5% (c) Co 10% (d) ZnO NRs.

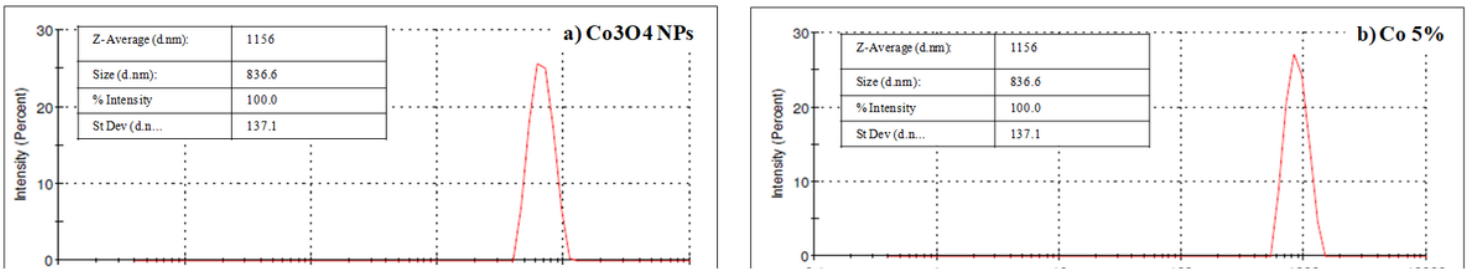

Figure 9

DLS particle size distribution of (a) Co_3O_4 NPs (b) Co 5% (c) Co 10% (d) ZnO NRs.

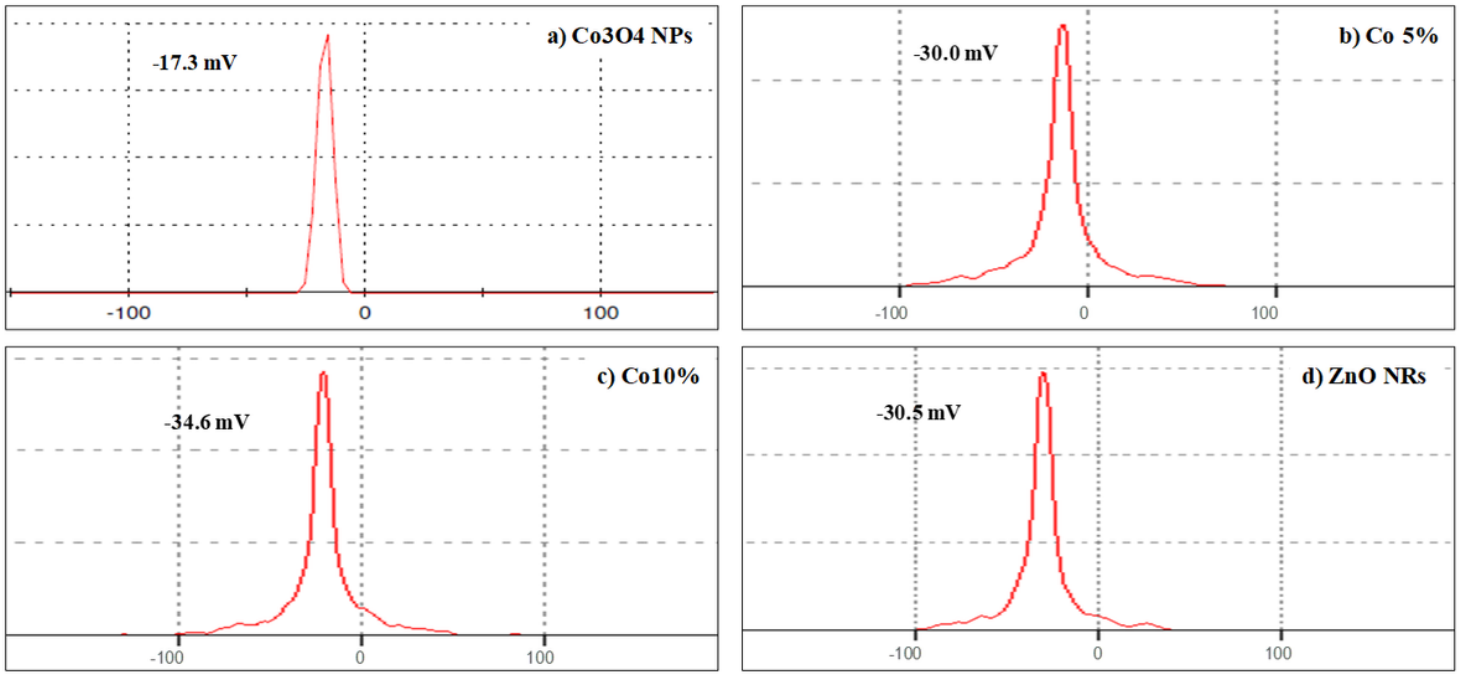

Figure 10

Zeta potential Distribution of (a) Co_3O_4 NPs (b) Co 5% (c) Co 10% (d) ZnO NRs.

Figure 11

TGA and DSC analysis of (a) Co_3O_4 NPs (b) Co 5% (c) Co 10% (d) ZnO NRs.

Figure 12

Comparative study antioxidant activity using DPPH and ABTS potential with different concentration of Co_3O_4 NPs, Co 5% nanocomposite, Co 10% nanocomposite and ZnO NRs. (n=3).

Figure 13

Anti-inflammatory effects of ZnO NRs, Co_3O_4 NPs, Co 10% and Co 5% nanocomposite assessed against A) Heat-induced egg albumin denaturation and B) RBC Stabilization of Leukocyte (%)